

Design and Analysis of Planar Photonic Band Gap Devices

V. Tabatadze · A. Bijamov Jr · D. Kakulia ·
G. Sapparishvili · D. Kakulia · R. Zaridze · Ch. Hafner ·
D. Erni

Received: 10 March 2008 / Accepted: 22 August 2008 /
Published online: 5 September 2008
© Springer Science + Business Media, LLC 2008

Abstract The need for a highly efficient numerical simulation platform for designing photonic band gap (PBG) structures is outlined in the context of various functional device topologies. In this paper we therefore introduce the Method of Auxiliary Sources (MAS) as a semi-analytical, frequency-domain method for computational optics, which has already proven its accuracy and efficiency in various other fields of electrodynamics. The proposed software package provides an easy-to-handle approach to full-wave analysis of two-dimensional (2D) PBG circuits, PBG-based antennas as well as to dense-integrated optics components that contain optical waveguides, scatterers, resonators and other functional elements. Experimental verifications of the numerical results have been conducted along large-scale prototypes in the microwave frequency range for several device topologies.

Keywords Photonic crystals · Photonic devices · Filter · Waveguide · Diplexer · Circulator

1 Introduction

Photonic crystal (PhC) devices have attracted a great deal of interest because of the intrinsic functionalities they offer for ultra-dense integrated optics. The underlying principle is

V. Tabatadze (✉) · A. Bijamov Jr · D. Kakulia · G. Sapparishvili · D. Kakulia · R. Zaridze
Laboratory of Applied Electrodynamics, Tbilisi State University, 3, Chavchavadze Ave., Tbilisi, Georgia
e-mail: vasil_i_tabatadze@yahoo.com

R. Zaridze
e-mail: rzaridze@laetsu.org

C. Hafner
Laboratory for Electromagnetic Fields and Microwave Electronics, ETH Zurich, 8092 Zurich,
Switzerland
e-mail: christian.hafner@ifh.ee.ethz.ch

D. Erni
General and Theoretical Electrical Engineering (ATE), Faculty of Engineering,
University of Duisburg-Essen, 47048 Duisburg, Germany
e-mail: daniel.erni@uni-due.de

referred to as photonic band gap (PBG), as it was first discovered in optical applications (for theoretical foundations cf. [1–4]). The scaling properties of electrodynamics, however, supports the presence of band gaps not only in visible light, but also in e.g. the lower part of the frequency spectrum, often referred as electromagnetic band gap (EBG). Band gap-based devices in the THz regime are prone to solve numerous problems, such as e.g. providing planar approaches to miniaturization beyond the quasi-optical scheme, and functional elements based on particular dispersion features and/or dense localization. Compact realizations of microwave devices such as waveguides, filters, mixers, splitters, become feasible when PhCs, i.e., PBG or EBG structures are used as underlying core elements. Referring to the realm of photonics the increase in operating frequency poses a challenge to the fabrication technology, as well as to the prior design procedure, because small sub-wavelength features have to be handled in material systems that are subject to both, losses and material dispersion.

In general PhC devices consist of an artificial crystal made of different dielectrics or metals arranged on a regular lattice, where functionality is inserted using appropriately arranged defects. Such defects are typically characterized as confined areas where symmetry-breaking is introduced into the crystal, either by emphasizing or omitting specific lattice sites (i.e. the inclusion of different material or the omission of a lattice node). According to the lattice symmetry of the PhC the dispersion diagram comprises spectral gaps (i.e. the PBG or EBG) denoting a forbidden frequency regime with no allowed propagation states, whereas at frequencies adjacent to the gap signals can pass through. In contrast to ordinary absorbing media, the PhC virtually do not dissipate energy when e.g. lossless media are involved and pure 2D lattice symmetry is assumed. Hence, electromagnetic energy accumulation and power combining defines an inherent functionality of the underlying PhC scheme, meaning that PhC structures are prone to mold incident wave fields in the spectral as well as in the spatial domain.

In general, the experimental investigation of PhC structures is rather expensive, time consuming and, in some cases, even impossible as the fabrication and the accurate measurements are both defining very challenging ventures. Therefore, computer aided design based on highly efficient numerical simulation methods become vitally important. The need for efficiency is underpinned especially when the influence of fabrication tolerances on the device performance has to be predicted, using e.g. a Monte-Carlo or a sensitivity analysis. In addition experimental investigations can be simplified if they are carried out along large-scale prototypes in the microwave frequency range.

In the remainder of the paper we present several PhC devices such as a power splitter, a mixer, filters, and a circulator arranged as building blocks for larger circuit topologies. These devices were designed by means of an efficient numerical field analysis, based on the Method of Auxiliary Sources (MAS), where the latter is outlined in Section II. In general, realistic PhC devices are planar three-dimensional (3D) structures. Their numerical full-wave analysis may become very time-consuming. As a proof of concept, one therefore tends works with 2D models, i.e., models with cylindrical symmetry that extends to infinity in the z -direction. Hardware modeling in the microwave regime has already proven its ability to provide reliable reference data for correspondingly downscaled planar PhC devices [5]. Referring to planarity our hardware model therefore consists of two conducting parallel planes perpendicular to the z -axis, for which the PhC structures are introduced in between. This kind of “sandwiched” Lecher-type structure is capable to maintain the symmetry inherent to a pure 2D PhC analysis, while making the experimental evaluation of 2D PhC circuits pretty straightforward. Note, that the distance between the plates is wavelength dependent and should be usually kept between half and a quarter of the

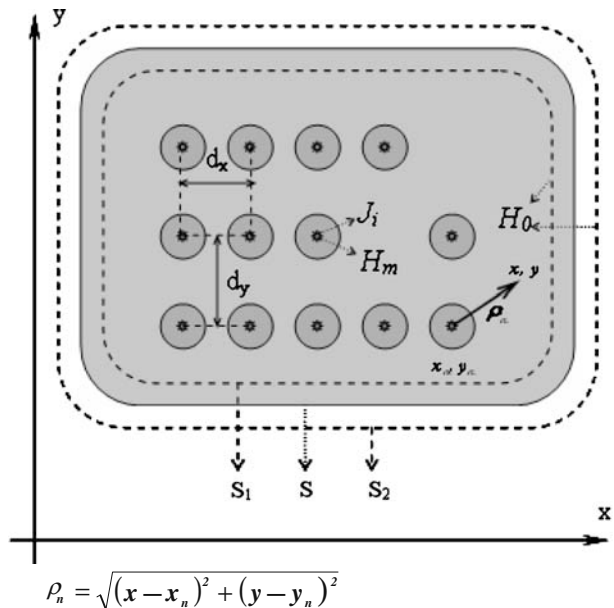
operating wavelength. The analysis and the design of the various PhC devices are outlined in Section III together with the corresponding microwave measurements. A numerical assessment of the production constraints is elucidated in Section IV in the framework of both, the PhC antenna and the PhC circulator; and, finally, some conclusions are drawn in Section V.

2 Method of auxiliary sources

The PhC structures to be analyzed in the following consist of a dielectric rectangular host, which encompasses a periodical arrangement of dielectric or metallic rods (cf. Fig. 1). The functionality of the devices is mainly obtained by the implementation of particular defects that are introduced by replacing certain rods or changing the parameters of some existing ones. The excitation of the structure is performed using a linear current flowing along a cylindrical wire that can be applied at any arbitrary position within the crystal lattice. This copes well with experiments, where a straight wire fed by an external current source is accordingly placed in the hardware model. The resulting electrodynamic problem is then solved using the Method of Auxiliary Sources (MAS) [6], which is also known as the method of fictitious sources [7]. In a general framework MAS may also be considered as generalized multipole technique [8], which is based on lowest-order multipoles, such as zero order multipoles or monopoles in 2D, and first order multipoles or dipoles in 3D. Furthermore, MAS can be understood as the electrodynamic extension of the charge simulation method [9] known from electrostatics.

Since 2D PhC structures are solely analyzed in this paper, we will restrict our further elucidations to 2D MAS. As displayed in Fig. 1 the entire 2D dielectric space is split into several piecewise homogeneous domains D_i : the outer space, the inner crystal domain outside the rods defining the lattice host, and the proper area inside the rods.

Fig. 1 The MAS computational window with (x,y) denoting the coordinates of the observation point whereas (x_m) are the coordinates indicating the position of the n^{th} rod. S is a dielectric surface; S_1 and S_2 are inner and outer auxiliary surfaces.



The electromagnetic field inside each domain D_i is then approximated by a superposition of elementary fields stemming from auxiliary sources that are distributed strictly outside the corresponding domain. Usually, the auxiliary sources are arranged along auxiliary lines (e.g. S_1 and S_2) that follow the boundary (e.g. S) of the domain:

$$U_{D_i} = \sum_{v=1}^{N_i} C_{vi} H_0^{(1)}(k_i r_{vi}), \quad (1)$$

Where

$$k_i = \frac{2\pi\sqrt{\varepsilon_i\mu_i}}{\lambda}$$

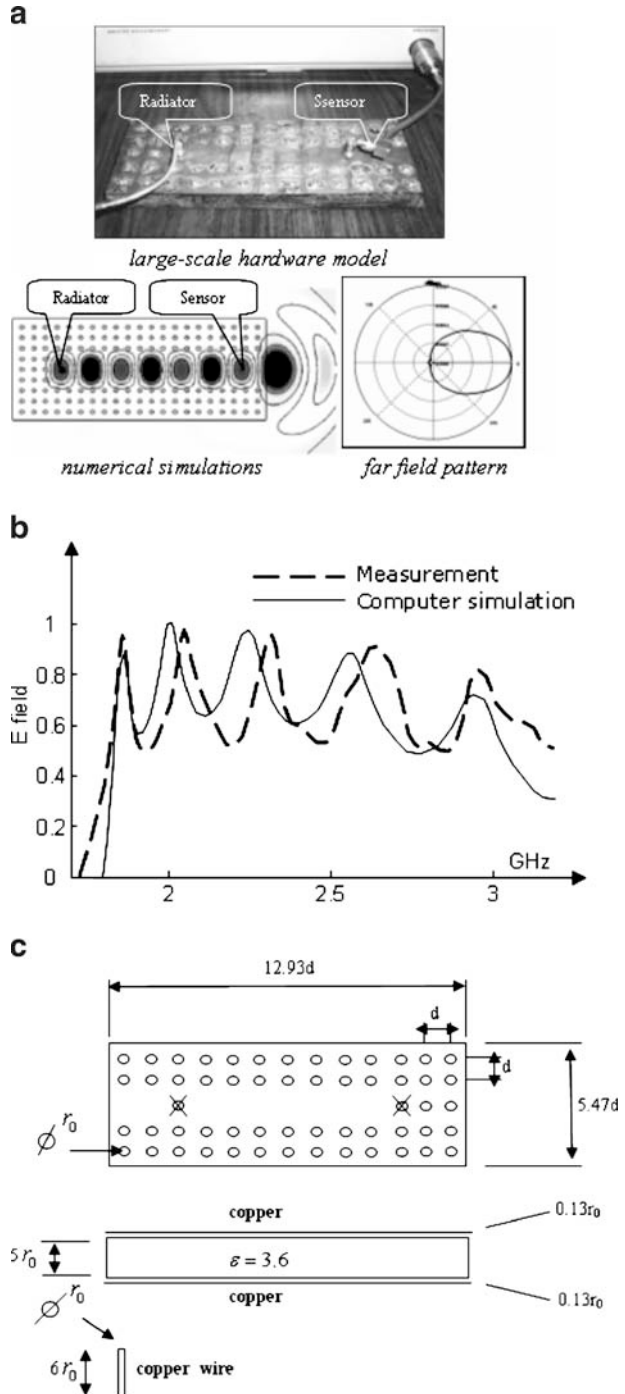
is the wave number within D_i and r_{vi} denotes the distance between observation point and auxiliary source. In the case of perfectly conducting (PEC) rods no field is expected inside and, thus, the corresponding sources are omitted. For simple PhC structures with circular rods shown in Fig. 1, one may replace a) the auxiliary sources that model the field inside the circle by a single Bessel expansion J of order θ up to i and b) the auxiliary sources that approximate the scattered field outside the circle by a multipole expansion H of order θ up to m , usually with $i = m$ [10].

The unknown expansion coefficients C_{vi} have to be determined by enforcing the boundary conditions for the tangential field components on the surfaces of all domains. This is carried out using point matching or collocation techniques, which lead to a linear system of equations in the complex domain. Unlike other widely used computational techniques like the FDTD method a distinct advantage of MAS lays in the existence of an explicit error measure provided by the matching error on the boundaries. All the subsequent analysis has been carried out while keeping the relative error below 5%. Due to the semi-analytic feature of MAS the accurate computation of 2D PhC structures is very fast yielding simulation times in the order of few seconds per frequency point on a state-of-the-art PC. Consequently, MAS turns out to be best suited for numerical structural optimization including PhC design scenarios, which are guided e.g. by advanced global search heuristics [11–14]. The MAS is provided as a fully equipped simulation platform, with an easy-to-handle graphic user interface, which, e.g., allows the straightforward introduction of the geometry together with the direct placement of the sources and sensors for excitation and exploration purposes [6].

3 Computer simulation & results

In the following we present different PhC devices based essentially on one and the same sandwich-like experimental setup that consists of two metallic plates with the dielectric structure in between. A PhC structure is formed here by a set of metallic cylindrical rods arranged on a rectangular lattice, as illustrated in Fig. 1. At microwave frequencies, the metallic rods may be considered as perfect electric conductors (PEC), which allows us to neglect the field inside, and, thus considerably reduces the computational effort. In a first design step, the lattice constants d_x and d_y must be chosen in such a way that the PBG coincides with the desired operation bandwidth [11]. As a second step, functionality is introduced by the proper placement of defects in the PhC, which are represented by vacancies, namely by the absence of rods in some specific lattice sites.

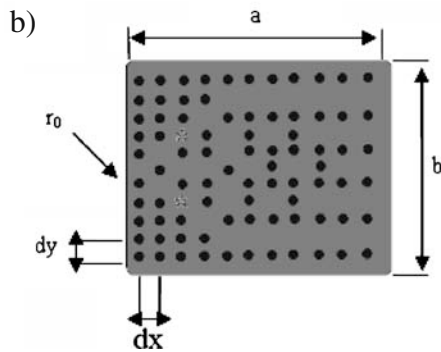
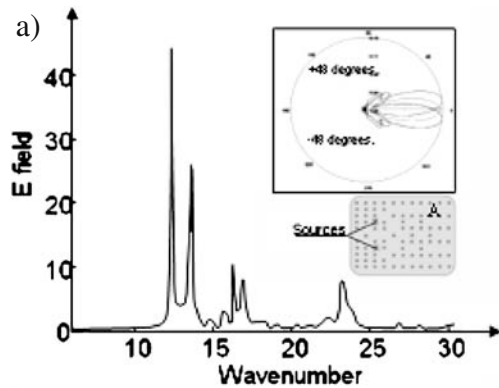
Fig. 2 a): PhC W3 waveguide section b): numerical/experimental verification of the open ended PhC W3 waveguide section. Spectral response of the electric field strength from 1.95 GHz to 3.0 GHz. c): $d/r_0=5$, Frequency range: from 1.95 GHz to 3.0 GHz.



3.1 PhC waveguide and radiation from the open waveguide termination:

One of the most simple and most important defect structures is the line defect, where a line of missing rods is forming a distinct waveguide channel. Figure 2 shows a W3 waveguide that is obtained when three parallel lines of rods are removed. The PhC device consists of a W3 waveguide of finite length, with one end within the PhC (i.e. short termination) and the other end forming an open termination on the opposite side. Guided waves may be excited, for example, using a simple coaxial cable feed near the short termination. In our simulation, this feed is represented by an imposed current at the corresponding position. The W3 waveguide channel supports nearly lossless wave propagation evolving into a directed radiation pattern at the waveguide’s open end [cf. Fig. 2(a)]. The spectral response of the field inside the waveguide [cf. Fig. 2(b)] displays resonant features stemming from the distinct reflections at both ends of the waveguide channel. It’s worth mentioning, that despite the strong confinement of the PhC waveguide, the open termination imposes a significantly lower power reflection than a corresponding open termination of a conventional rectangular waveguide. This is due to the very specific nature of the line defect, where the outmost defect at the open termination of the PhC waveguide could be viewed as a single radiator that is fed by the adjacent defects, namely by the waveguide channel, yielding a considerably large radiation efficiency, and, thus, the unexpected low power reflection. The spectral responses in Fig. 2(b) also depict a comparison between our

Fig. 3 a) Simulated characteristics of the beam-steering antenna (radiated field’s value in the A point versus wave number, configuration and far field pattern. b) Geometrical dimensions of beam-steering antenna.



$$\epsilon = 12; n = \sqrt{\epsilon} = 3.46; dx = 11.3 \text{ Ro.}$$

$$dy = 7.7 \text{ Ro. } a = 12dx, b = 83.9dx,$$

Frequency range 4.8 - 5.2 GHz.

simulation and the experimental data. The results are in good agreement over a wide frequency range of 1.95 GHz–3.0 GHz. Besides the errors inherent to the microwave equipment and the measurement setup, the small spectral deviations are explained by the inaccuracy of both, the dielectric parameters and the shape of the PhC structure owing to fabrication uncertainties of the prototype. The normalized geometrical dimensions of the underlying channel waveguide are provided in Fig. 2(c).

3.2 PhC beam-steering antenna:

High-speed beam-steering without involving mechanical motion is highly desirable because of the lack of mass inertia. As we will show here PBG-based antennas are prone to provide pure electronic (or optical) steering schemes. The PhC-based beam-steering antenna consists of defects that are arranged to form several intersecting channels starting from two feed points and evolving into five coupled parallel channel waveguides as illustrated in Fig. 3(a). The working principle is based on the phase difference between the two sources, which is then equally distributed among the outgoing waveguide channels to provide the necessary phase shift for the corresponding beam direction. By means of controlling the phase shift (ranging up to 48°) between the channels one may achieve steering angles up to 30° . Furthermore, when applying source signals of slightly different wavelengths one inherently gets a time periodic pivoting of the beam according to the beat frequency yielding the desired scanning features. The beam-steering can be easily controlled and achieves fast steering rates. Figure 3(b) represents normalized geometrical dimensions of the analyzed beam-steering antenna.

3.3 PhC power splitter:

Generally speaking, PhC devices are PhCs enabling different functionalities, where the latter is associated to different distributions of defects according to the underlying circuit

Fig. 4 Diplexer model.

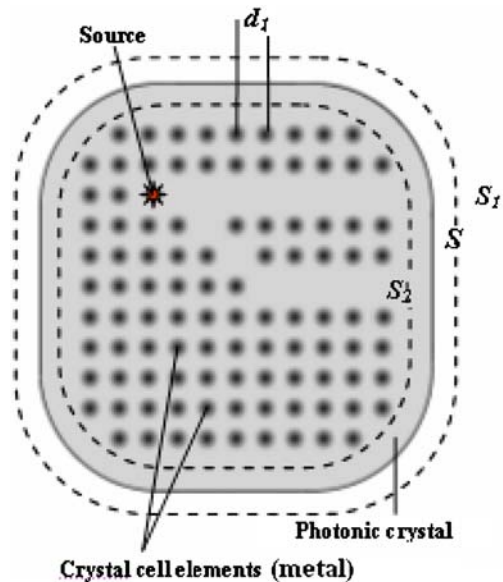
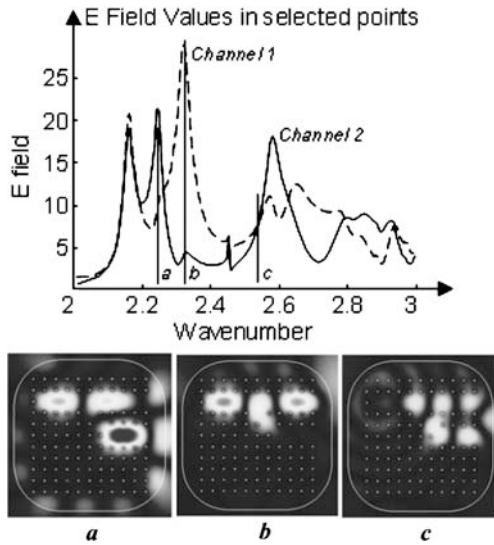


Fig. 5 PBG-based diplexer: numerical simulations and operation characteristics: dependence of the field distribution in channels on excitation frequency. (a, b, c).



topology. In particular for PhC devices any such design is neither intuitive nor straightforward. It mostly involves computer-guided design scenarios based e.g. on sensitivity analysis or on numerical structural optimization [12–14]. On the system level the situation may become less severe, because the distinct confinement properties of the channel waveguides enable the PhC scheme to provide a kind of modularity. As a consequence, the setup of a complex PhC circuit, which relies on the proper arrangement of basic PhC building blocks, may start to resemble a classical engineering scenario, involving experience, intuition and particular skills. A corresponding example will be presented in sub-section G.

At the next PhC building block we show in Fig. 4 a simple frequency selective power splitter, which consists of a single feed and two output channels. By altering the operating frequency, it is possible to control the total amount of power emitted from both channels (cf. Fig. 5). Besides such diplexer operation (cf. operation frequency *a*) and *b*) there are frequencies (e.g. the one labeled *c*) where the device operates as a power splitter. Both operation principles are further elucidated in the following two sub-sections addressing the design of a power combiner and a diplexer.

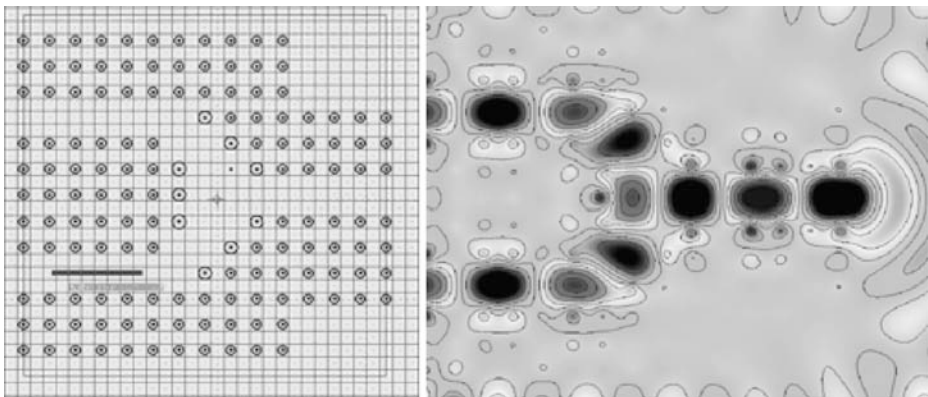


Fig. 6 PhC power combiner (left) and computer simulation of the electric field strength (right).

3.4 PhC power combiner:

In Fig. 6, we consider a device, which is virtually identical to the power splitter; however, it combines the incoming signals instead of splitting them into two parts. Figure 6 depicts the structure and the corresponding computer simulation for a simple PhC power combiner. If the incoming flux is distributed equally between the two incoming ports, 79% of the power is transmitted through the single output channel, whilst 17% is reflected from the coupling area. Thus, only 4% of power is dissipated laterally. It's worth mentioning that even a symmetric, virtually lossless three-port exhibits a residual power reflection due to fundamental reasons.

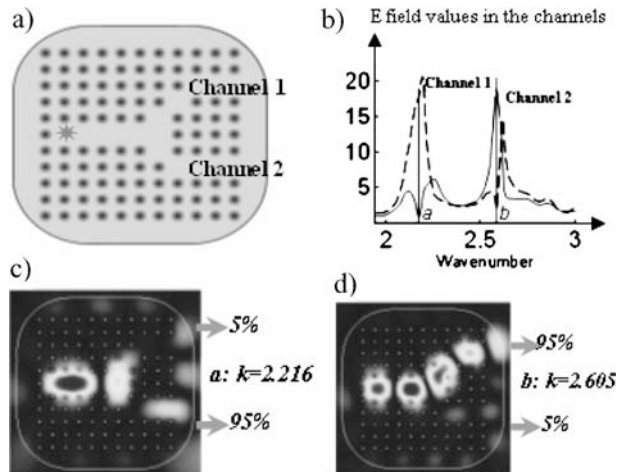
3.5 PhC diplexer:

According to Fig. 7 two different waveguide channels are introduced into the PhC to form a diplexer. Each channel has been created by eliminating rods in a slightly different manner, leading to an asymmetry in the output channel geometry, which, due to emerging resonant properties is responsible for the unique filtering characteristics of the system. Figure 7 displays the spectral response of the diplexer's transmission behavior. The dashed and solid lines represent the field strength at the output of channel 1 and channel 2, respectively. For narrowband operation the diplexer shows an isolation of nearly 26 dB. Please note, that due to the specific diplexer response proper broadband designs are only achievable along full-blown numerical structural optimization, where both diplexer bands are subject to optimization. The degradation of the diplexer response due to manufacturing inaccuracies is further discussed in Section IV.

3.6 PhC circulator:

The circulator presented here may be termed as one of the most intriguing PhC structures [cf. Fig. 8 (a)]. As in conventional realizations the PhC circulator encompasses three ports enabling wave propagation according to the following transmission scheme: channel 1 - channel 2, channel 2 - channel 3, and channel 3 - channel 1. In conventional isolators the operational non-reciprocity is introduced with nonlinearity, whereas here the apparent non-reciprocity rests on the interrelation between symmetry properties and the emergent field

Fig. 7 a) PGB filter b) Frequency characteristic for two channels output (measured during simulation) c) Near field distribution at wave length $k=2.216$ when the field goes through second channel d) Near field distribution at wave length $k=2.605$ when the field goes through first channel.



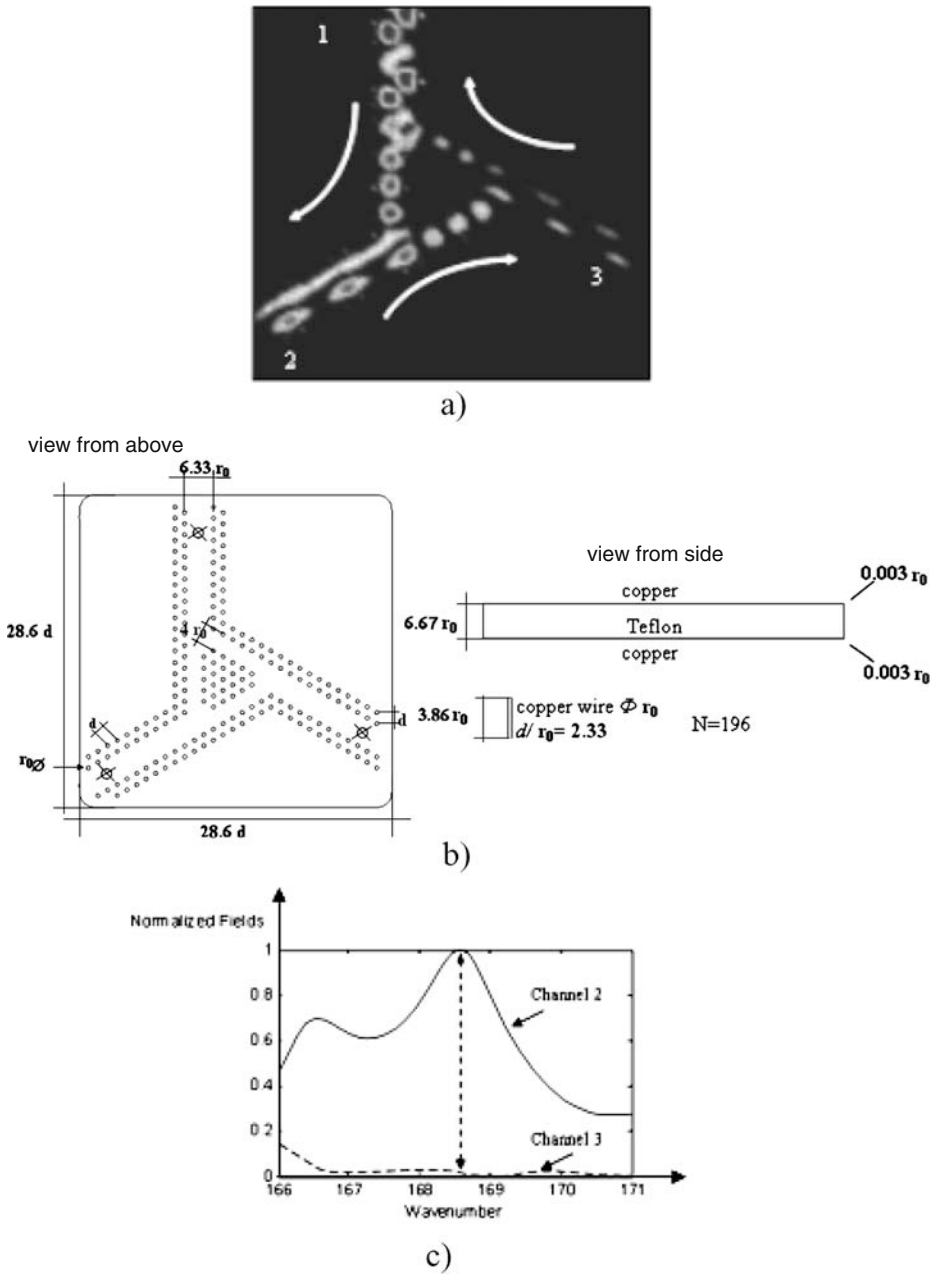


Fig. 8 a): PBG-based circulator and numerical simulation b) The normalized geometrical dimensions of circulator c) Performance of the PhC circulator: The upper line shows the field amplitude in the output channel 2 of the device, and the lower one shows the amplitude in the output channel 3, whereas the circulator is fed through channel 1. (the spectral response is simulated).

states in the underlying structure given in Fig. 8 (a). Hence, the PhC circulator proposed here is based on linear elements only. Unlike to the prior PhC devices, it relies on a hexagonal lattice of metallic rods embedded into a dielectric host material with a large permittivity. The three accessing channels consist each of a W2 PhC waveguide that is connected to a triangle-shaped area inside the structure, which itself is framed by three W1 PhC waveguide sections [cf. Fig. 8(b)].

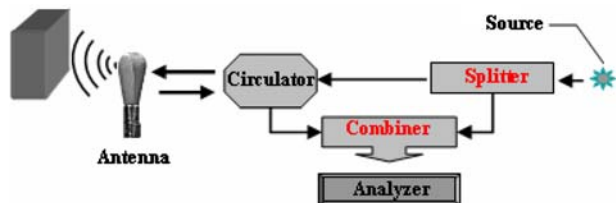
If a signal is applied to the channel 1, over 90% of the input power will be emitted through channel 2 at the expense of a residual signal in channel 3. From the reciprocity theorem we would, though, expect in the reciprocal situation a reversed signal transmission starting from channel 2 back to channel 1, which is obviously not the case. Instead, the outgoing wave will emerge from channel 3. What looks like mysticism at first sight, is explicable along two reasoning as follows. First, any symmetric, lossless, and perfectly matched three-port circuit has to be non-reciprocal and in particular turns out to be a circulator. The second reasoning addresses the proper mechanisms inside the PhC circulator. The crucial idea behind the PhC circulator is that its geometrical dimensions are selected in such a way, that the waves following path 1-3 and path 1-2-3 reach both the output channel 3 with opposite phases, yielding therefore the aforementioned output signal in channel 2. As phase relations are involved this working principle applies only to a relatively narrow frequency range, while outside of this range the circulator loses its characteristic properties. The field simulations in Fig. 8(a) reveal that the wave's modes in channel 2 differs from the modes in channel 1, thus, the wave passing through the circulator structure is carried by a changing set modes. The working principle of the PhC circulator, and, hence the apparent non-reciprocity is therefore rooted in the multi-mode behavior of the structure in conjunction with the structure's symmetry. Imposing simple time reversal, which is tantamount to correspondingly adjusting the phases of all involved mode fields, would expose reciprocity in its very straightforward sense. Figure 8(c) displays the spectral response of the PhC circulator's performance if the structure is excited through the waveguide channel 1: The upper curve shows the normalized field amplitude at the output of channel 2, and the lower curve depicts the same quantity at the output of channel 3. The circulation takes place at the resonance frequency so the operating frequency range is pretty narrow. Please note that an increase in bandwidth is only achievable with the inclusion of non-linear elements.

3.7 Example of a functional PhC circuit:

A more complex PhC circuit for remote exploration of a dielectric body's surface is presented in Fig. 9. It employs all the discussed PhC building blocks and its operation is rather straightforward, as already denoted in sub-section C.

The field from the source is equally split after the splitter into two signals, where the first one (i.e. the reference signal) is directly forwarded to the power combiner. The second signal, however, is introduced into the circulator, after which it is applied to the antenna.

Fig. 9 Schematics depicting the functionality of the PhC circuit for remote exploration of the dielectric body surface.



The antenna structure is represented by an open channel waveguide termination with a slightly modified, lens-like output facet. From there the electromagnetic fields are impinging the dielectric surface and reflected back while carrying all the essential structural information. The reflected waves are then captured by the antenna, and forwarded to the circulator, being assigned to a different path. So, at this stage, there is only negligible coupling between the incoming and outgoing waves in the circulator. The signal then moves towards the combiner (cf. sub-section D), where it is combined with the reference signal, and both signals are then led to the analyzer which provides us with the information regarding potential cracks, stretches or other structural features of the dielectric surface. The overall topology of the PhC circuit for is displayed in Fig. 10. The bandwidth of the overall device tends to be narrow, thus it is best suited to work at a fixed operation frequency.

4 Simulation of manufacturing precision

Referring to the PhC devices presented so far, our conceptual studies have revealed that the PhC scheme offers a high degree of functionality confined to exceedingly small length scales in the wavelength range. The price to pay is a very challenging fabrication technology that has to reconcile sub-wavelength precision with the inherent process inaccuracies. As a matter of fact it is virtually impossible to get rid of process variations, such as random deviation in the shapes and positions of the rods and discrepancies between implied and actual material parameters. It is thus, of economical and practical interest to predict the influence of these uncertainties on the nominal behavior of the PhC device in order to specify the tolerances in the device performance. The MAS algorithm was therefore adapted to investigate the influence of such parameter variations on the device performance in a Monte-Carlo like scheme. Here, the software randomly alters the selected parameters within user-specified constraints, providing the opportunity to estimate the device behavior under real-world conditions.

For example, let us consider first the beam steering antenna with its quite narrow resonance peak as depicted in Fig. 3(a). Here we have altered the positions and sizes of the

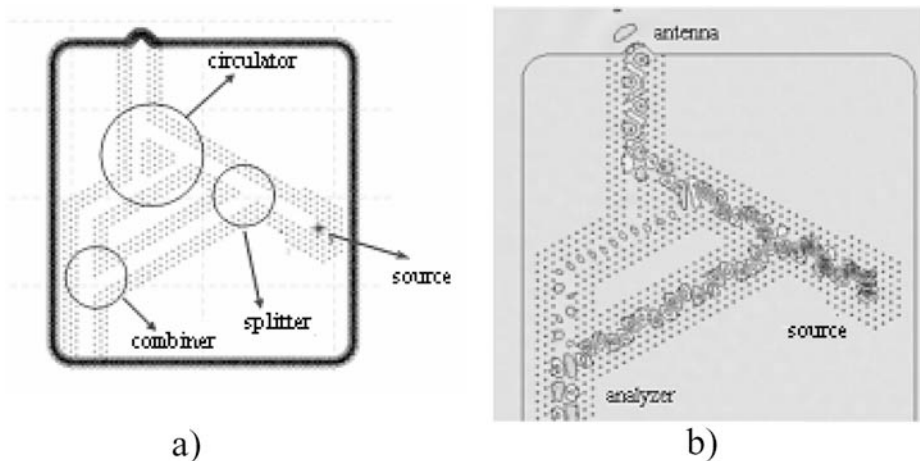
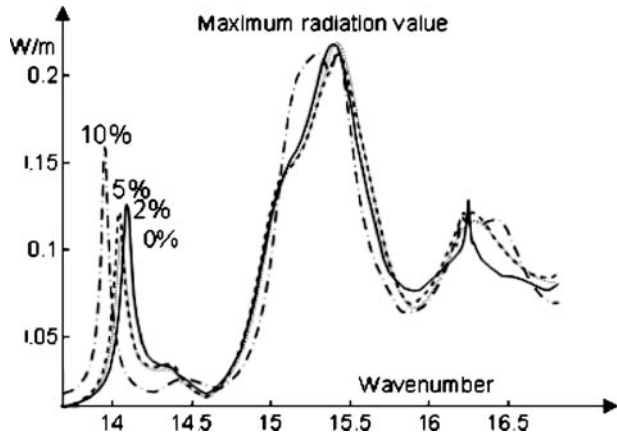


Fig. 10 Computer simulation of the integral scheme for remote exploration of dielectric bodies. a) Crystal geometry b) Near field distribution.

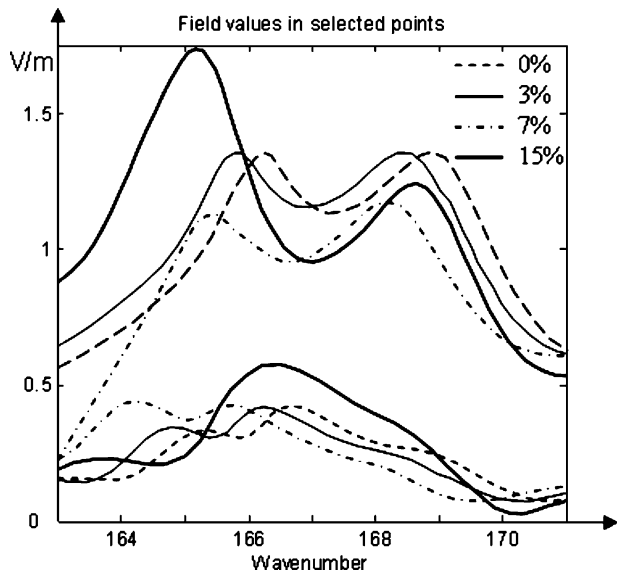
Fig. 11 Radiated power versus wave number for the beam-steering antenna, for different ranges of manufacturing inaccuracy.



rods within ranges of 2%, 5% and 10%, respectively. The resulting frequency responses for the corresponding scenarios (2%, 5%, and 10%) are depicted in Fig. 11, providing snapshots from the corresponding sets of different random configurations together with the unperturbed case. It's worth noting that for the PhC antenna fabrication tolerances up to 5% are quite acceptable, while larger variations may have a significant impact on the operating frequency and, hence, completely changes the intrinsic field distribution. Moreover this comes along with a widening of the resonance peaks, which corresponds to a reduced Q -factor (Fig. 11).

The second example encompasses the PhC circulator as shown in Fig. 12. The intrinsic electromagnetic fields strongly deviate from their resonant distributions, and the entire system loses its nominal properties. Nevertheless, relative inaccuracies up to 7% do not dramatically change the operation conditions, while e.g. values around 10%-15% start to show a significant impact on the circulator performance.

Fig. 12 E_z Field values in two middle points of the circulator in second and third channels versus wave number ($1/m$) for different ranges of manufacturing inaccuracy. If the inaccuracy is greater than 10% the deviation from normal-mode operation is high and the results are unpredictable.



5 Conclusions

Based on 2D MAS simulations we have proposed several PhC devices (i.e. waveguides, antennas, mixers, filters, and circulators) that may be used as building blocks for ultra-compact photonics circuits. As the structures were designed without much optimization effort, there is still room for further improvement. Despite the proposed new device concepts experimental verifications of the numerical results have been conducted along large-scale prototypes in the microwave regime for several device topologies. Furthermore, fabrication issues and device stability versus process variations were discussed in the framework of a Monte-Carlo-type analysis. Optimized real-world designs according to given specifications of either PhC building blocks or complex PhC systems have inevitably to rely on numerical structural optimization [12–14]. Under these circumstances, the proper design of functional 3D PhC structures using appropriate numerical 3D models still remains a very challenging task, which has to be subject to future investigations.

Acknowledgements This work was supported by the Swiss National Science Foundation in the framework of project NFP-SCOPE5-7GEPJ065551.

References

1. E. Yablanovich, “Inhibited spontaneous emission in solid-state physics and electronics”. *Phys. Rev. Lett.* **58**, 2059–2062 (1987).
2. J. Joannopoulos, R. Meade, and J. Winn, *Photonic Crystals: Modeling the flow of light* (Princeton University Press, 1995).
3. H. Benisty, “Modal analysis of optical guides with two-dimensional photonic band-gap boundaries”. *J. Appl. Phys.* **79**, 7483–7492 (1996).
4. A. Chutinan, M. Okano, and S. Noda, “Wider bandwidth with high transmission through waveguide bends in two-dimensional photonic crystal slabs”. *Appl. Phys. Lett.* **80**, 1698–1700 (2002).
5. G.-A. Chakam, A. Rumberg, and W. Freude, Modeling photonic band gap structures in the microwave region near 10 GHz,” *Int. Top. Meeting on Microwave Photon. MWP 2002*, Nov. 5–8, pp. 333–336, Awaji, Japan, 2002.
6. R. Zaridze, G. Bit-Babik, K. Tavzarashvili, N. Uzunoglu, and D. Economou, “Wave Field Singularity Aspects Large-Size Scatterer and Inverse Problems.” *IEEE Transactions on AP*, vol.50, No. 1, January 2002, pp. 50–58.
7. G. Tayeb, and S. Enoch, “Combined fictitious-sources-scattering-matrix method”. *J. Opt. Soc. Am. A* **21**, 1417–1423 (2004).
8. Ch. Hafner, *The Generalized Multipole Technique for Computational Electromagnetics*. (Artech House Books, Boston, 1990).
9. X. Liu, Y. Cao, and E. Wang, Numerical simulation of electric field with open boundary using intelligent optimum charge simulation method, *IEEE Trans. On Magnetics*, vol. 42, no.4, April 2006, pp 1159–1162.
10. Ch. Hafner, *Post-Modern Electromagnetics: Using Intelligent Maxwell Solvers*. (John Wiley & Sons, Chichester, 1999).
11. D. Karkashadze, R. Zaridze, A. Bijamov, Ch. Hafner, J. Smajic, and D. Erni, MAS and MMP Simulations of Photonic Crystal Devices. Extended Papers Proceedings of Progress In EM Research Symposium (PIERS-2004). March 28–31, 2004, Pisa, Italy. pp. 29–32.
12. J. Smajic, C. Hafner, and D. Erni, “Optimization of photonic crystal structures”. *J. Opt. Soc. Am. A* **21** (11), 2223–2232 (2004)November.
13. Ch. Hafner, X. Cui, J. Smajic, and R. Vahldieck, “Efficient procedures for the optimization of defects in photonic crystal structures”. *J. Opt. Soc. Am. A* **24**(4), 1177–1187 (2007)April.
14. J. Smajic, Ch. Hafner, X. Cui, and R. Vahldieck, “Numerical optimization of photonic crystal structures”. *J. of Computational and Theoretical Nanoscience* **4**(3), 675–685 (2007)May.